Power Electronics and Drives
Volume 10(45), 2025 DOI: 10.2478/pead-2025-0017

Power Electronics and Drives

A Grid-Compatible Adaptive Charging Strategy for Bidirectional On-Board EV Chargers with SOC and Thermal Integration

Research Paper

Omkar Malleni[1,2,*], Vijaya Kumar M.[3]

[1]Research Scholar, Department of Electrical & Electronics Engineering, Jawaharlal Nehru Technological University Anantapur, Anantapuramu, Andhra Pradesh, 515002, India
[2]Lecturer, Department of Electrical & Electronics Engineering, Government Polytechnic Anantapur, Andhra Pradesh, 515002, India
[3]Professor, Department of Electrical & Electronics Engineering, Jawaharlal Nehru Technological University Anantapur, Anantapuramu, Andhra Pradesh, 515002, India

Received: 10 June, 2025; Received in the revised form: 03 August, 2025; Accepted: 04 August, 2025

Abstract: This paper presents a novel adaptive charging strategy for a three-phase bidirectional on-board electric vehicle (EV) charger. The charger system enables seamless grid-to-vehicle (G2V) and vehicle-to-grid (V2G) operations while enhancing battery longevity and grid compatibility. It integrates real-time battery state of charge (SOC) and temperature feedback, with a predictive first-order thermal model to dynamically adjust charging parameters, mitigating degradation. Featuring a three-phase LCL filter, an AC–DC converter and a buck-boost DC–DC converter, the charger employs proportional-integral (PI) control for the AC–DC converter and an adaptive controller for the DC–DC converter. It achieves low total harmonic distortion (THD) of 1.33% (G2V) and 1.7% (V2G), 98.3% efficiency and a 30% reduction in charging time (5 h for 20%–80% SOC) compared with conventional methods. MATLAB/Simulink simulations confirm robust performance under sensitivity analysis, demonstrating stability. The system's unified control framework, combining SOC-based mode switching, thermal derating and harmonic suppression, outperforms existing methods, offering a scalable solution for smart grid integration and sustainable EV charging infrastructure.

Keywords: *electric vehicle • grid to vehicle • vehicle to grid • adaptive control • total harmonic distortion*

1. Introduction

The escalating global adoption of electric vehicles (EVs), projected to exceed 20 million units by 2024, has highlighted significant limitations in the existing charging infrastructure. The key challenges include the sparse deployment of charging stations, the degradation of battery health due to suboptimal charging protocols and the increasing demand on the grid from a growing EV fleet. Conventional charging systems typically employ static charging profiles that cannot adapt to the dynamic requirements of the battery, leading to excessive thermal generation and a reduction in battery lifespan and efficiency. Furthermore, the emergence of vehicle-to-grid (V2G) technology, which enables bidirectional power transfer between EVs and the grid for applications, such as peak shaving and frequency regulation, introduces additional complexities related to effective bidirectional power flow management and the mitigation of harmonic distortion. To address these concerns, there is a growing demand for sophisticated charging systems that can optimise battery health, enhance grid stability and improve charging efficiency.

To address these challenges, numerous studies have explored enhanced charging technologies. Bidirectional chargers, enabling both grid-to-vehicle (G2V) and V2G operations, alongside high-frequency switching power electronic control techniques and advanced bidirectional converter topologies, are pivotal for effective load balancing,

* Email: omkarmalleni@gmail.com

peak shaving and renewable energy integration within smart grid architectures (Sethuraman and Rudhramoorthy, 2024; Thangavel et al., 2023). Models of batteries with thermal awareness have been explored to minimise overheating concerns during high-power charging (Shahjalal et al., 2021). To achieve power quality standards, the need for harmonic suppression employing LCL filters and sophisticated current control was emphasised (Ahmadi et al., 2019; Haque et al., 2023; Omkar and Vijaya Kumar, 2024). Adaptive charging algorithms are designed to enhance the efficiency of the system (Gong et al., 2018; Hammerschmitt et al., 2024). Charger configurations have been modelled with compliance to the IEEE 519 harmonic distortion standards (Acharige et al., 2023; Bera et al., 2022) and empirical assessments of power quality performance in urban distribution networks with substantial EV adoption have been conducted (Zdraveski et al., 2022). State of charge (SOC) estimate approaches utilising Kalman filters and neural networks have been implemented (Danko et al., 2019), as well as comprehensive analyses of grid interconnection protocols and bidirectional charging strategies (Etemesi et al., 2024; Han et al., 2020). Comparative analyses consistently emphasise the imperative for intelligent, thermally regulated adaptive charging systems to overcome current limitations (Pradhan et al., 2023; Rivera et al., 2021).

Despite these advancements, conventional systems face challenges in balancing fast charging with thermal safety, precisely regulating SOC and assuring bidirectional power quality. Traditional chargers are not designed to dynamically adjust charging current and voltage based on real-time temperature and SOC. An adaptive charging technique for a three-phase bidirectional on-board charger is presented in this paper to address these limitations. The system uses a thermal model for predictive control and dynamically modifies charging behaviour based on real-time battery SOC and temperature feedback. The proposed method maintains total harmonic distortion (THD) within IEEE 519 standards, enhancing thermal safety, minimising charging duration and ensuring grid compliance. This approach improves fast, safe and efficient charging and discharging operations in smart grid systems by integrating intelligent monitoring with real-time control. This paper is structured as follows: Section II describes the methodology with mathematical models, Section III presents simulation results, Section IV provides a comparative analysis and Section V draws the conclusions.

2. Methodology

The proposed adaptive charging methodology integrates intelligent control and thermal modelling within a three-phase bidirectional on-board charger system.

2.1. System topology

Figure 1 illustrates the complete structure of a three-phase bidirectional EV charger system. It comprises a three-phase grid connection that delivers AC power through an LCL filter to eliminate harmonics. The filtered AC is then transformed to DC via a three-phase AC–DC converter. This DC power is stabilised by a DC link capacitor and then regulated by a bidirectional buck-boost DC–DC converter. The DC–DC stage charging and discharging of the battery is managed using an adaptive charging control technique with temperature and SOC-based regulation. Control systems are implemented for both converters to ensure regulated power flow, grid compliance, and support for G2V and V2G operation.

2.2. Mathematical modelling

The ideal grid source voltage and current are v_a, v_b, v_c and i_a, i_b, i_c, where L and R denote the circuit inductance and resistance. v_{dc}, i_{dc}, C is the DC link voltage, current and capacitance, respectively.

By applying KVL and KCL, the system model can be expressed as follows (Han et al., 2020):

$$\begin{aligned} v_a &= L\frac{di_a}{dt} + Ri_a + u_{an} + u_{no} \\ v_b &= L\frac{di_b}{dt} + Ri_b + u_{bn} + u_{no} \\ v_c &= L\frac{di_c}{dt} + Ri_c + u_{cn} + u_{no} \\ c\frac{dv_{dc}}{dt} &= i_{dc} - i_L \end{aligned} \tag{1}$$

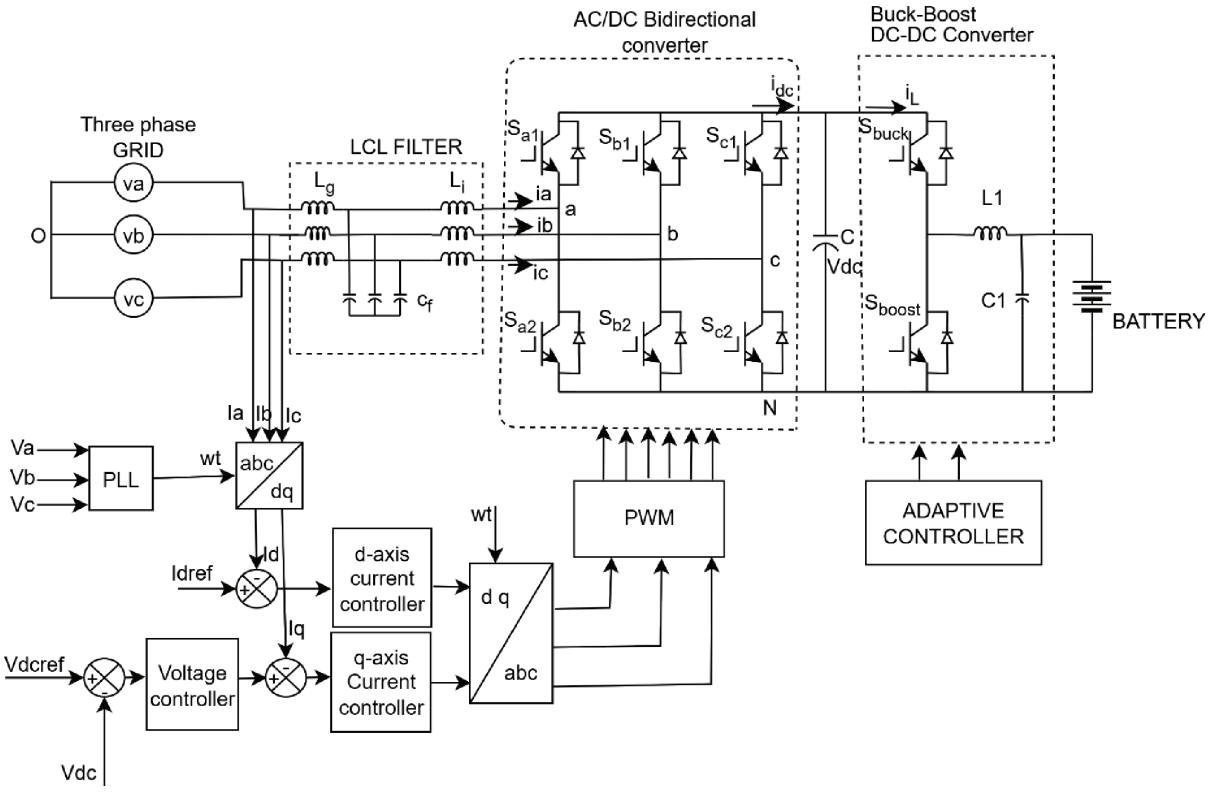

Figure 1. Block diagram of three-phase bidirectional on-board charger. PLL, phase-locked loop.

where u_{no} is the voltage between *N* and *O*, and u_{an}, u_{bn} and u_{cn} are the voltages between the converter legs and neutral point *O*. Switching function is $S_k = 1$ when switches S_{a1}, S_{b1}, S_{c1} are on and S_{a2}, S_{b2}, S_{c2} are off, and $S_k = 0$ when switches S_{a2}, S_{b2}, S_{c2} are on and S_{a1}, S_{b1}, S_{c1} is off. Thus, u_k may be written as follows:

$$u_k = u_{kn} + u_{no} = s_k u_{dc} + u_{no} \qquad (k = a,b,c) \tag{2}$$

$$\begin{aligned} v_a &= L\frac{di_a}{dt} + Ri_a + v_{dc}\left[s_a - \frac{1}{3}(s_a + s_b + s_c)\right] \\ v_b &= L\frac{di_b}{dt} + Ri_b + v_{dc}\left[s_b - \frac{1}{3}(s_a + s_b + s_c)\right] \\ v_c &= L\frac{di_c}{dt} + Ri_c + v_{dc}\left[s_c - \frac{1}{3}(s_a + s_b + s_c)\right] \\ C\frac{dv_{dc}}{dt} &= i_a s_a + i_b s_b + i_c s_c - i_L \end{aligned} \tag{3}$$

The equation is shown in an *a*, *b*, *c* system, but it is more appropriate to represent it in a stationary reference α, β frame as follows:

$$\begin{bmatrix} v_\alpha \\ v_\beta \end{bmatrix} = [M]\begin{bmatrix} v_a \\ v_b \\ v_c \end{bmatrix}, \tag{4}$$

$$\begin{bmatrix} v_a \\ v_b \\ v_c \end{bmatrix} = \frac{3}{2}[M]^T\begin{bmatrix} v_\alpha \\ v_\beta \end{bmatrix}, \tag{5}$$

$$\frac{3}{2}[M]^T = \begin{bmatrix} 1 & 0 \\ -\frac{1}{2} & \frac{\sqrt{3}}{2} \\ -\frac{1}{2} & \frac{\sqrt{3}}{2} \end{bmatrix}$$

where v_α, v_β are α, β frame quantities and v_a, v_b, v_c are stationary *a*, *b* and *c* frame quantities. The α, β frame is represented as follows:

$$\begin{aligned} v_\alpha &= L\frac{di_a}{dt} + Ri_a + s_a v_{dc} \\ v_\beta &= L\frac{di_b}{dt} + Ri_b + s_b v_{dc} \\ c\frac{dv_{dc}}{dt} &= \frac{3}{2}\left(i_a s_a + i_b s_b\right) - i_L \end{aligned} \tag{6}$$

The transition from the stationary (*α*, *β*) frame to the synchronous (*d*-*q*) frame, achieved through Park's transformation, aligns the reference frame with the grid's rotating magnetic field at angular frequency *ω*. This converts time-varying sinusoidal signals into steady-state DC signals, simplifying power control by decoupling active (*d*-axis) and reactive (*q*-axis) components and facilitating more effective voltage and current regulation as follows:

$$\begin{bmatrix} v_d \\ v_q \end{bmatrix} = [T]\begin{bmatrix} v_\alpha \\ v_\beta \end{bmatrix}, \tag{7}$$

$$[T] = \begin{bmatrix} \cos(w_o t) & \sin(w_o t) \\ -\sin(w_o t) & \cos(w_o t) \end{bmatrix},$$

$$\begin{bmatrix} v_\alpha \\ v_\beta \end{bmatrix} = [T]^{-1}\begin{bmatrix} v_d \\ v_q \end{bmatrix}, \tag{8}$$

$$[T]^{-1} = \begin{bmatrix} \cos(w_o t) & -\sin(w_o t) \\ \sin(w_o t) & \cos(w_o t) \end{bmatrix},$$

Where v_d, v_q are synchronous *d*-*q* frame quantities. Using Eqs (6) and (7) we can simplify the model as follows:

$$\begin{aligned} v_d &= L\frac{di_d}{dt} + Ri_d - w_o L i_q + s_d v_{dc} \\ v_q &= L\frac{di_q}{dt} + Ri_q - w_o L i_d + s_q v_{dc} \\ c\frac{dv_{dc}}{dt} &= \frac{3}{2}\left(i_d s_d + i_q s_q\right) - i_L \end{aligned} \tag{9}$$

Based on Eq. (9), Figure 2 represents a three-phase voltage source converter *d*-*q* synchronous reference model.

2.3. Design of filter components

The design of the LCL filter is crucial for ensuring power quality in the bidirectional charger system. The LCL filter comprises the converter-side inductance, grid-side inductance and a filter capacitor, and it is responsible for attenuating high-frequency switching harmonics introduced by the power converter. The grid-side inductance (Lg) plays a specific role in limiting the high-frequency current injected into the grid. It acts as a buffer that smoothens the current waveform and reduces electromagnetic interference (EMI). Additionally, Lg helps improve the stability of the control system, particularly under weak grid conditions, and assists in suppressing resonance by interacting

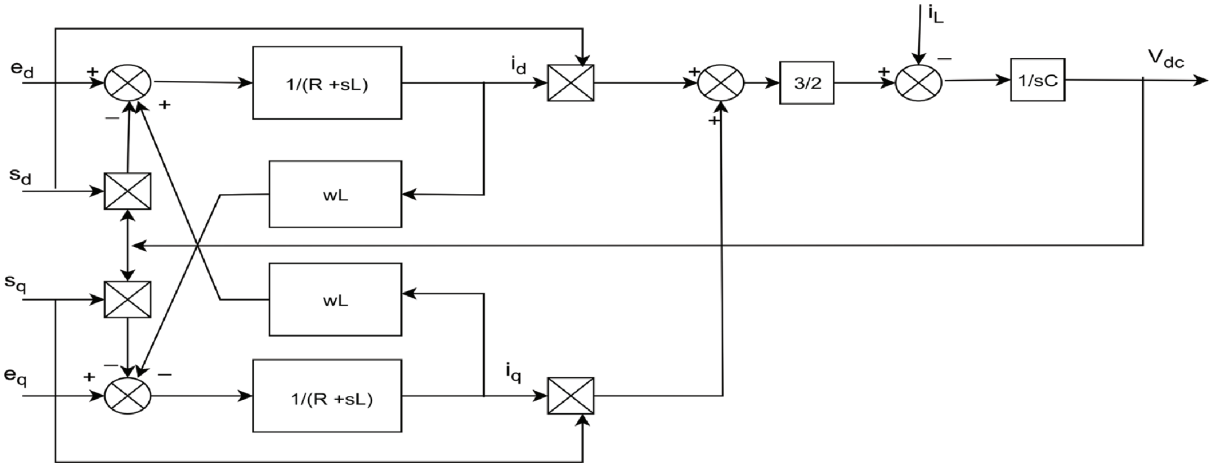

Figure 2. Synchronous *d-q* frame model of a three-phase converter.

with the filter capacitor. Its value must be carefully chosen to balance the filtering effectiveness and avoid excessive reactive power injection or resonant oscillations. The design of the filter is as follows:

$$\text{The base impedance } z_b = \frac{E_n^{\,2}}{P_n} \tag{10}$$

$$\text{The base capacitance } c_b = \frac{1}{w_g z_b} \tag{11}$$

Where P_n, E_n and w_g denote rated power, rated voltage and angular grid frequency, respectively.

The product of the base capacitance of the converter and the rate of reactive power absorption yields the filter capacitance (Omkar and Vijaya Kumar, 2024) as follows:

$$c_f = 5\%\ of\ c_b$$

$$C_f = 5\% \frac{p_n}{2\pi f_g E_n^{\,2}} \tag{12}$$

$$\text{The relation between the converter voltage and current is } V_{in} = L_i \frac{di_{in}}{dt}$$

$$\text{The maximum current ripple is } \Delta i_{\max} = \frac{V_{dc}}{6 L_i f_{sw}}$$

$$\text{The minimum value of the inductor on the converter side is } L_{i\min} = \frac{V_{dc}}{6 f_{sw} \Delta i_{\max}} \tag{13}$$

$$\text{The grid side inductance is } L_g = \frac{\sqrt{\frac{1}{k^2_a}} + 1}{C_f W^2 sw} \tag{14}$$

Where k_a is the attenuation factor and $f_{sw,}$ f_g and f_{res} stand for switching, grid and resonant frequencies, respectively.

It is crucial to note that a lower harmonic attenuation level leads to a decrease in current harmonics. Consequently, reducing *Ka* leads to a decrease in the THD of the grid current.

$$\text{The resonant frequency is } w_{res} = \sqrt{\frac{L_i + L_g}{L_i L_g c_f}} \tag{15}$$

After determining all LCL filter parameters, it is crucial to verify the resonance frequency to ensure that it does not align with low-order or high-order harmonics. This satisfies Eq. (16):

$$10 f_g \leq f_{res} \leq f_{sw}/2 \tag{16}$$

If the resonance frequency is <10 times the grid frequency, the capacitor value should be reduced. If it goes beyond half that threshold, the switching frequency or capacitor value can be increased. The LCL filter parameters were optimised to minimise THD while ensuring resonance damping and grid compatibility. The phase delay introduced by the LCL filter is compensated by using a phase-locked loop (PLL) within the synchronous *d-q* frame control, which aligns the reference frame with the grid voltage phase, ensuring synchronisation. Additionally, feedforward compensation is used to decouple the *d-q* axis currents, while the PI controller parameters are tuned to compensate for the phase delay caused by the LCL filter. The filter was tuned to achieve sufficient harmonic suppression without introducing resonant peaks, based on LCL filter design and IEEE 519 standards.

2.4. Adaptive controller

The core control logic dynamically adjusts the charging mode based on real-time battery metrics, including temperature and SOC. The adaptive controller uses the Coulomb counting method for SOC estimation, integrating battery current with an initial SOC, calibrated periodically to minimise drift (Danko et al., 2019).

Figure 3 depicts an adaptive charging control system that receives inputs from the battery SOC and temperature. These inputs are processed by the adaptive controller, which generates optimised reference signals for current and voltage. The controller ensures safe and efficient charging by dynamically adjusting these references based on real-time battery conditions.

Figure 4 illustrates a DC–DC adaptive controller that regulates battery charging using feedback from the output current. A PI controller processes the error between the reference and actual current, generating a PWM signal to drive either the buck or boost converter. The mode selection logic ensures appropriate operation based on current level comparisons, enabling efficient bidirectional energy flow. The Ziegler–Nichols tuning method is used to determine the PI controller parameters based on system oscillatory behaviour.

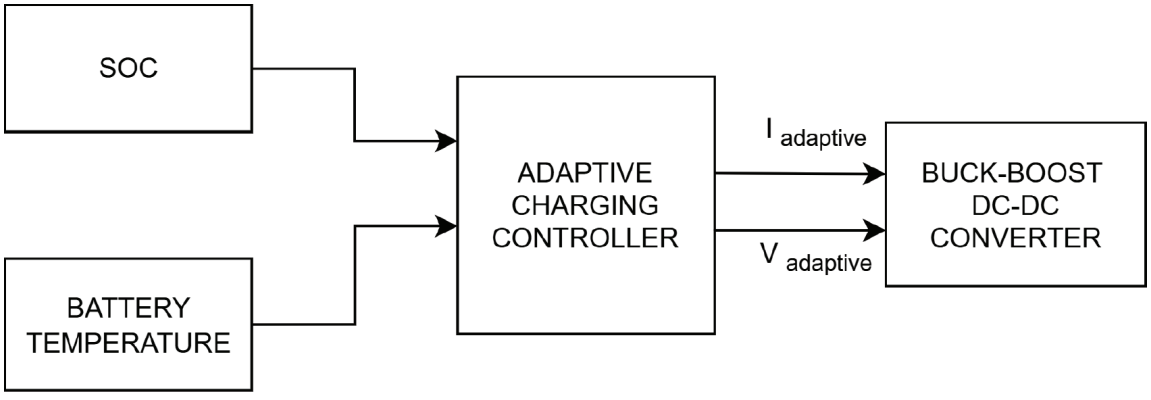

Figure 3. An adaptive charging controller block diagram. SOC, state of charge.

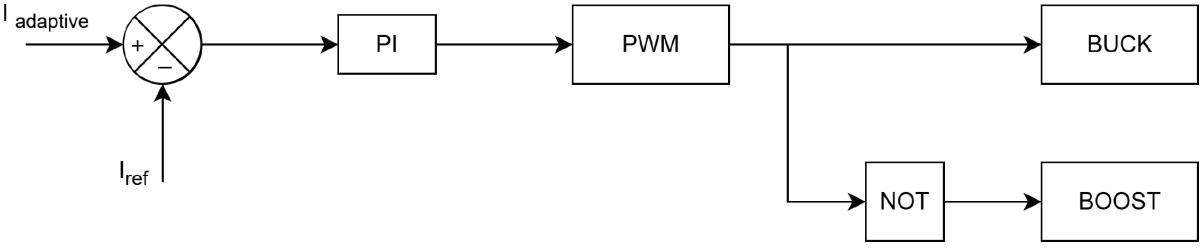

Figure 4. Controller for the buck-boost DC–DC converter.

The PI controller transfer function is given as $Gc(s) = Kp + \frac{Ki}{s}$ (17)

$$Gc(s) = Kp\left(1 + \frac{1}{T_i s}\right) \quad (18)$$

Proportional gain is $K_p = 0.45k_u$

Integral time constant is $T_i = \frac{T_u}{1.2}$

Integral gain is $K_i = \frac{K_p}{T_i}$

Where K_u = ultimate gain and T_u = ultimate period.

2.5. Thermal model integration

The battery's temperature change is governed by a first-order thermal differential equation:

$$C_{th} \cdot \frac{dT}{dt} = I^2 \cdot R_{int} - \frac{T - T_{amb}}{R_{th}} \quad (19)$$

Where: C_{th} = thermal capacitance (J/°C), R_{int} = internal resistance (Ω), R_{th} = thermal resistance (°C/W), T = battery temperature, T_{amb} = ambient temperature and I = battery current.

The internal resistance (R_{int}) is estimated using pulse current tests and voltage drop analysis across the battery terminals. Thermal capacitance (C_{th}) and thermal resistance (R_{th}) are derived from battery datasheet specifications.

Figure 5 illustrates the adaptive charging strategy for an EV battery system. It begins by measuring temperature and SOC. If SOC is <80%, the mode of constant current (CC) is activated; otherwise, mode of constant voltage (CV) is selected. In CC mode, the current is set to maximum unless the temperature exceeds the threshold, triggering current derating. The process continues to monitor SOC, and charging is terminated when 100% SOC is reached, ensuring safe and efficient battery operation.

3. Simulation Results

Table 1 outlines the key electrical and filter parameters of the bidirectional charger system, including a peak grid voltage of 325 V (peak), current of 25A (peak), frequency of 50 Hz and a switching frequency of 10 kHz. It also specifies the LCL filter components and battery-side capacitance, ensuring stable operation and effective harmonic mitigation.

Table 2 presents the key battery specifications (415 V, 50 kWh), which correspond to typical mid-range EVs and align with industry standards such as the Nissan Leaf and Hyundai Kona models. It also defines operating limits such as a maximum charging current of 30 A, an SOC transition threshold of 80% and a temperature limit of 45°C to ensure safe and efficient charging.

3.1. During G2V mode of operation

The proposed three-phase bidirectional on-board charger exhibits stable and efficient performance. The grid voltage (Figure 6a) maintains a smooth sinusoidal waveform with a 325 V peak (230 V RMS), indicating effective synchronisation. The grid current (Figure 6b) also shows sinusoidal waveforms with a balanced 25 A peak per phase, confirming harmonic mitigation and grid compliance.

Battery voltage (Figure 6c) rises steadily during CC mode, transitioning to CV mode at 400 V. Charging current (Figure 6d) starts at 30 A in CC mode and decreases during CV mode to ensure safety. The SOC (Figure 6e) increases rapidly by up to 80% in CC mode and then gradually under CV, ensuring faster yet safe charging. Charging power (Figure 6f) peaks at 12 kW near 80% SOC, followed by a gradual decrease in CV mode. FFT

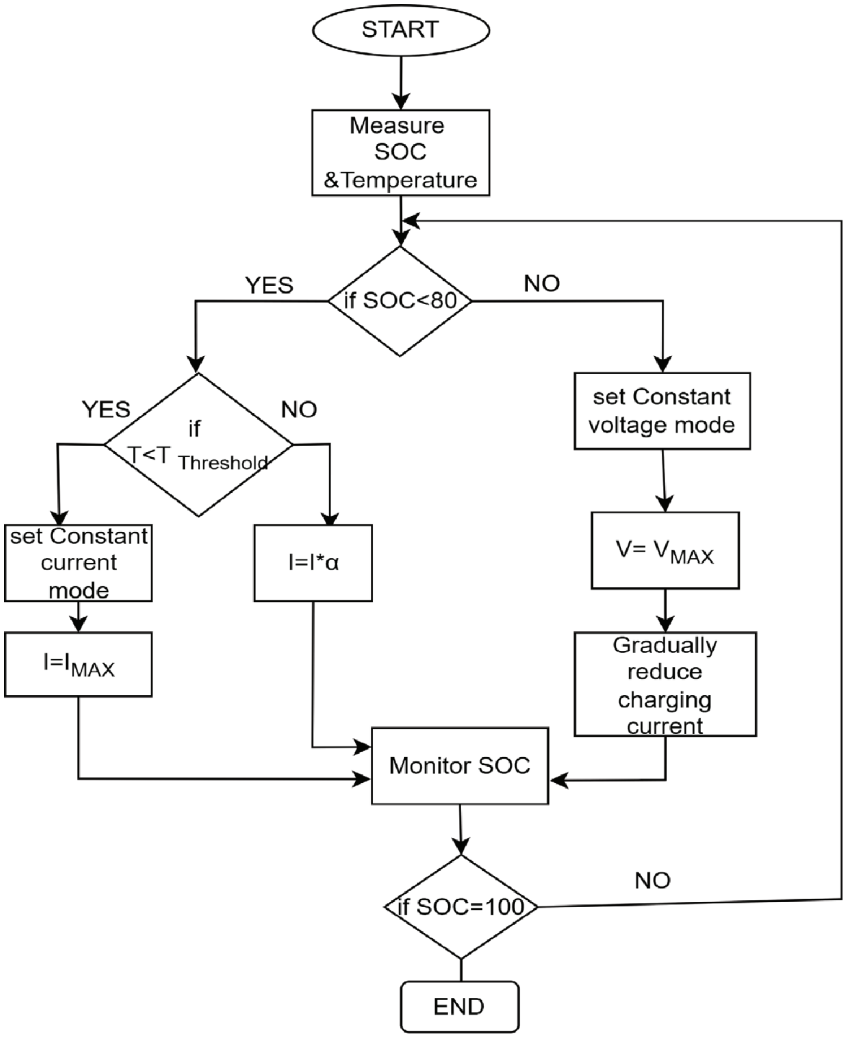

Figure 5. Flow chart for an adaptive controller. SOC, state of charge.

Table 1. Parameters of the system.

Parameter	Value
Grid voltage	325 V
Grid current	25 A
Grid frequency	50 Hz
Switching frequency	10 kHz
DC-link voltage	800 V
LCL filter inductance (each side)	5 mH
LCL filter capacitance	30 μF
DC link capacitance	5,600 μF

analysis (Figure 7a) shows a grid current THD of 1.33%, FFT analysis (Figures 7b and 7c) reveals a grid current THD of 1.51% and 1.23% at a grid inductance value of 4.5 mH and 5.5 mH. FFT analysis (Figures 7d and 7e) indicates a grid current THD of 1.48% and 1.27% at a grid voltage of 370 V and 460 V. It shows high power quality, confirming compliance with IEEE 519 standards. These results validate the effectiveness of the adaptive charging algorithm in optimising charging speed, safety and grid performance.

Table 2. Battery specifications.

Parameter	Value
Battery rated voltage	415 V
Maximum charging current	30 A
Rated capacity	50 kWh
Initial SOC	20%
SOC threshold (CC CV)	80%
Internal battery resistance	0.1 Ω
Temperature limit	45°C

CC, constant current; CV, constant voltage; SOC, state of charge.

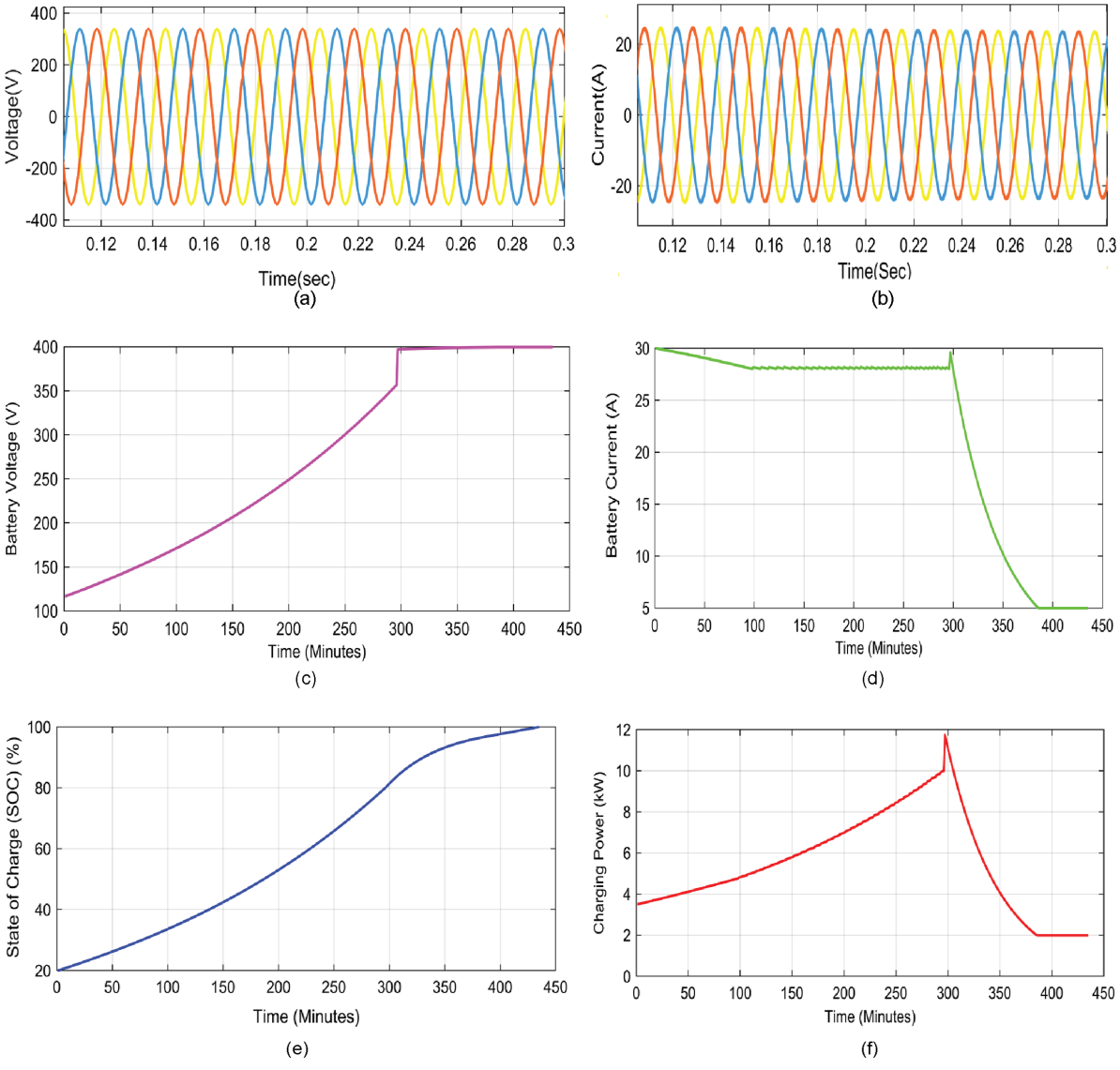

Figure 6. Three-phase bidirectional on-board charger performance during G2V mode: (a) Grid voltage, (b) Grid current, (c) Battery voltage, (d) Battery current, (e) Battery SOC and (f) Charging power. G2V, grid-to-vehicle; SOC, state of charge.

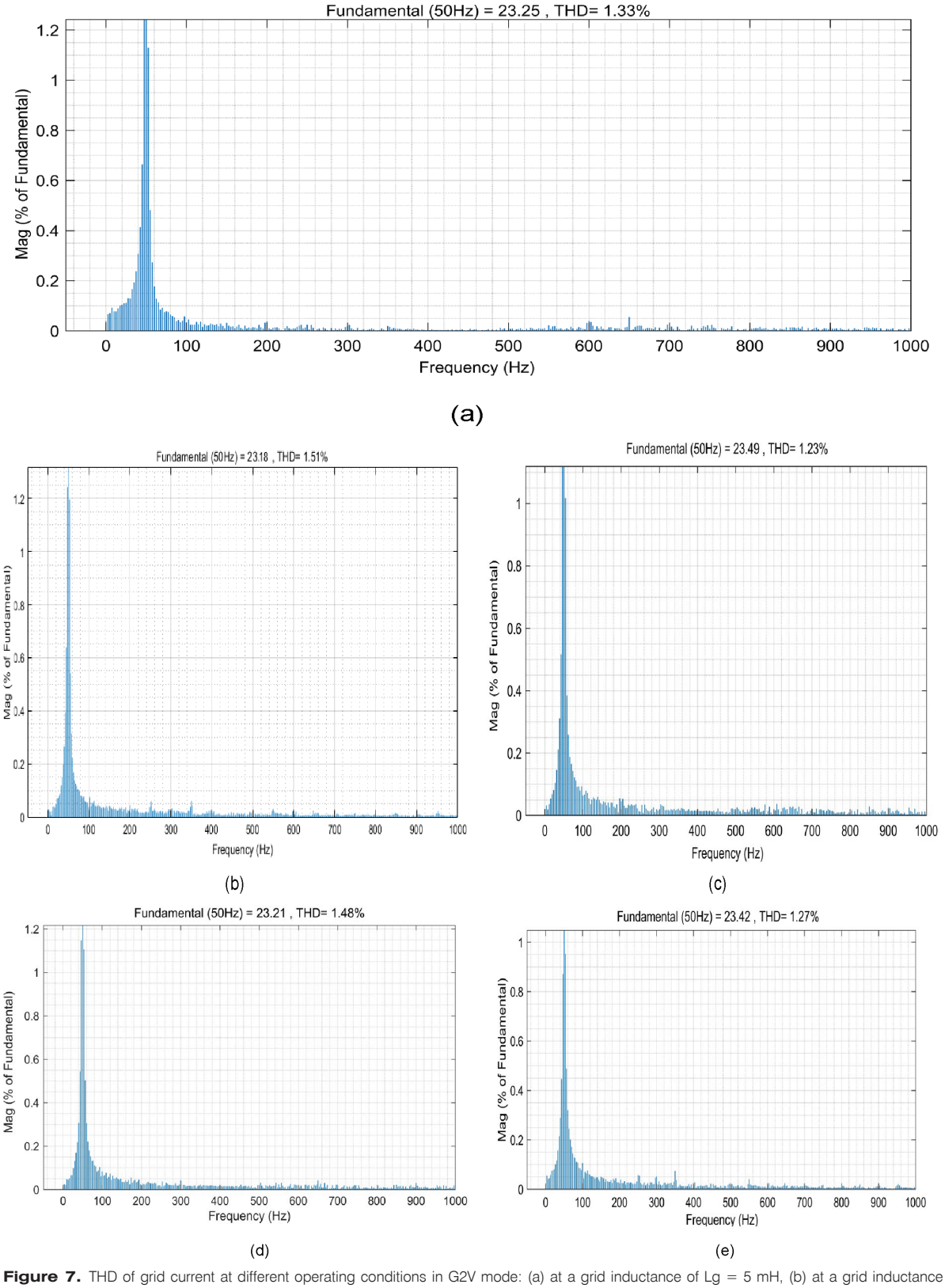

Figure 7. THD of grid current at different operating conditions in G2V mode: (a) at a grid inductance of Lg = 5 mH, (b) at a grid inductance of Lg = 4.5 mH, (c) at a grid inductance of Lg = 5.5 mH, (d) at a grid voltage of 370 V and (e) at a grid voltage of 460 V. G2V, grid-to-vehicle; THD, total harmonic distortion.

3.2. During V2G mode of operation

In V2G operation, the proposed bidirectional charger demonstrates stable and compliant power delivery. The voltage waveform (Figure 8a) and current waveform (Figure 8b) are sinusoidal with 325 V and 25 A peak, respectively, confirming proper synchronisation and low-distortion power injection into the grid. The battery voltage (Figure 8c) begins at 415 V and gradually decreases as discharging progresses, while the current (Figure 8d) remains steady at 30 A, ensuring consistent power transfer. The SOC (Figure 8e) exhibits a controlled linear decline, reflecting a safe and efficient discharge process governed by adaptive control logic. Discharging power (Figure 8f) shows initially peaking and then decreasing gradually with SOC, preventing deep discharge and preserving battery health. FFT analysis (Figure 9a) reveals a low THD of 1.7%; Figures 9b and 9c reveals a grid current THD of 2.10% and 1.62% at a grid inductance value of 4.5 mH and 5.5 mH; Figures 9d and 9e indicates a grid current THD of 1.92% and

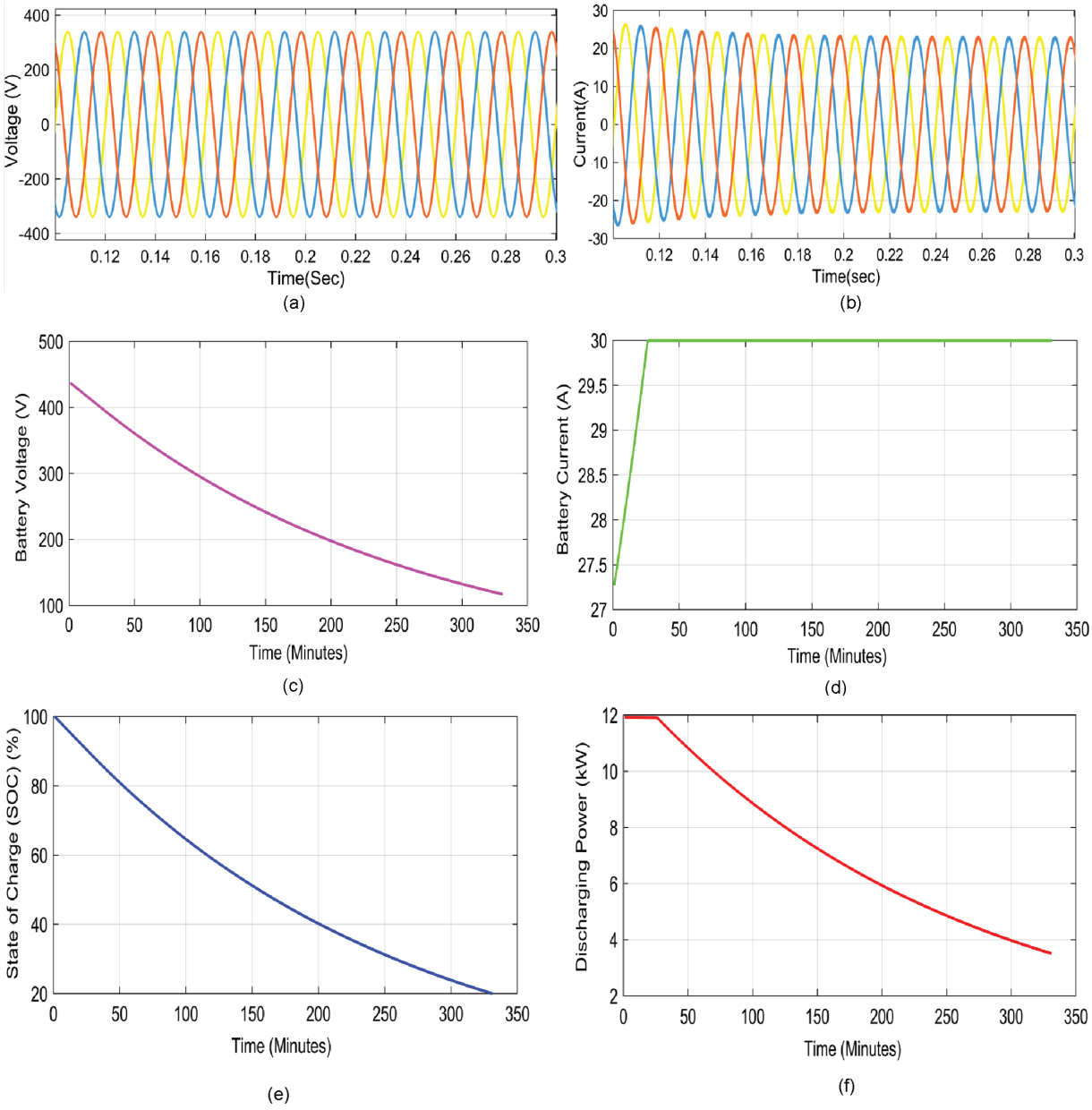

Figure 8. Three-phase bidirectional on-board charger performance during V2G mode: (a) Grid voltage, (b) Grid current, (c) Battery voltage, (d) Battery current, (e) Battery SOC, and (f) Discharging power. SOC, state of charge.

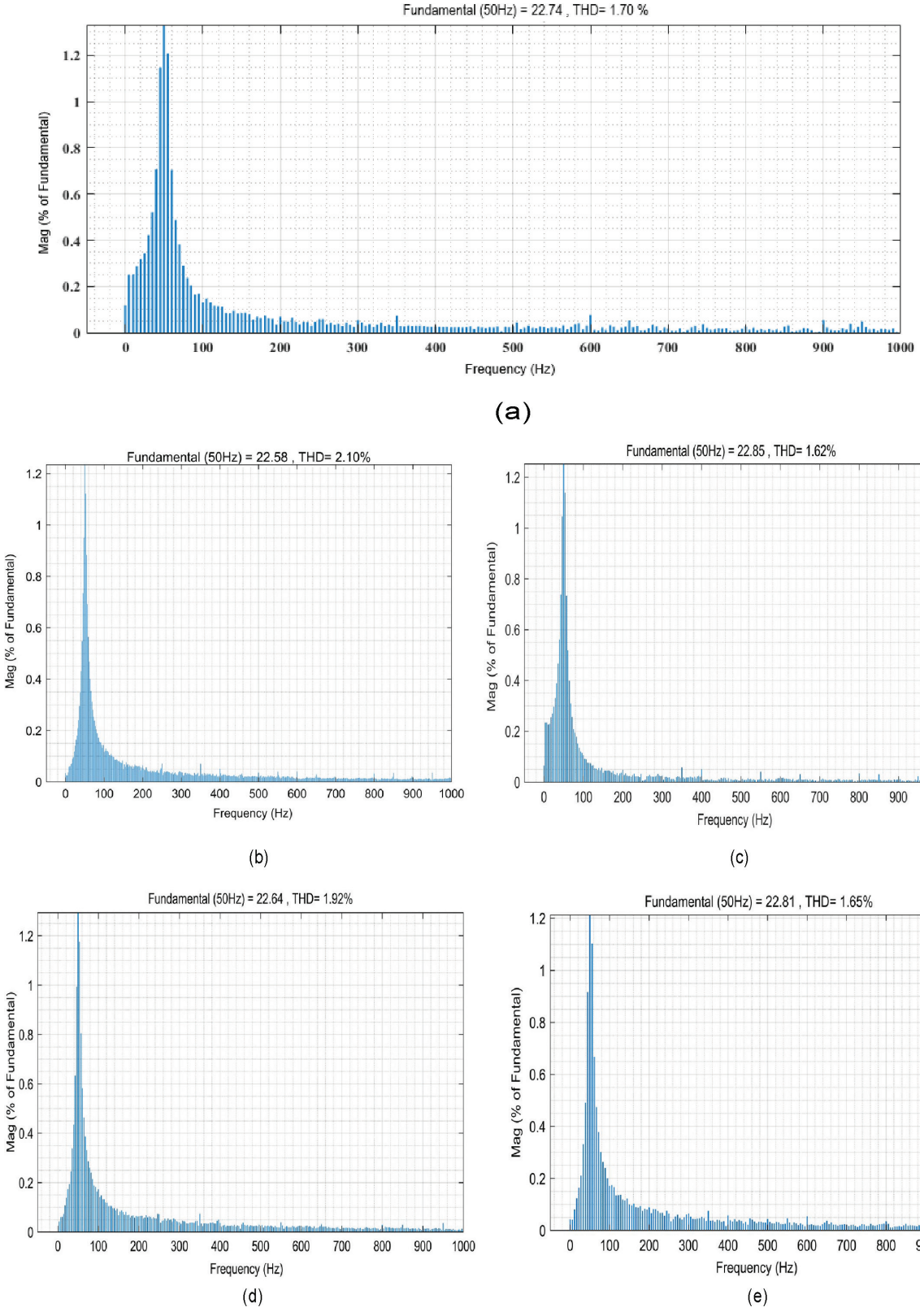

Figure 9. THD of grid current at different operating conditions in V2G mode: (a) at a grid inductance of Lg = 5 mH, (b) at a grid inductance of Lg = 4.5 mH, (c) at a grid inductance of Lg = 5.5 mH, (d) at a grid voltage of 370 V and (e) at a grid voltage of 460 V. THD, total harmonic distortion; V2G, vehicle-to-grid.

Table 3. Sensitivity analysis with parameter variation.

Parameter	Variation	THD (G2V)	THD (V2G)
Lg (mH)	4.5–5.5 (±10% change in grid side inductance)	1.23%–1.51%	1.62%–2.1%
Grid voltage (V)	370–460 V (±10% change in grid voltage)	1.27%–1.48%	1.65%–1.92%

G2V, grid-to-vehicle; THD, total harmonic distortion; V2G, vehicle-to-grid.

1.65% at a grid voltage of 370 V and 460 V, indicating high power quality. These findings confirm the effectiveness of the suggested adaptive V2G technique to ensure efficient energy delivery, grid stability and battery longevity.

3.3. Sensitivity analysis

Table 3 shows a sensitivity analysis with parameter variation to assess the robustness of the proposed adaptive charging system by varying critical parameters such as grid-side inductance (Lg) and grid voltage levels. The THD was measured during both G2V and V2G operations under these variations. For Lg values ranging from 4.5 mH to 5.5 mH, the THD in G2V mode varied between 1.23% and 1.51%, while in V2G mode it ranged from 1.62% to 2.1%. Similarly, with grid voltage variations from 370 V to 460 V, the G2V THD remained within 1.27%–1.48%, and V2G THD ranged from 1.65% to 1.92%. These values are well within IEEE 519 harmonic limits, demonstrating that the system remains stable and grid-compliant even under significant variations, confirming its robustness to practical disturbances and parameter uncertainties.

4. Analysis and Discussion

The simulation findings show that the suggested adaptive charging technique for a three-phase bidirectional on-board charger works effectively in both G2V and V2G modes. In G2V operation, the controller smoothly transitions from CC to CV mode at 80% SOC, achieving fast charging with a peak power of 12 kW while preserving battery health. Grid voltage and current remain sinusoidal (325 V, 25 A peak per phase), with THD around 1.33%. During V2G mode, the battery discharges at a steady 30A initially, tapering as SOC decreases. The THD improves to 1.7%, demonstrating efficient harmonic suppression and stable grid power injection. The low THD in both modes ensures minimal harmonic distortion, reducing stress on grid infrastructure and enabling compliance with IEEE 519 standards, critical for urban charging stations with high EV penetration. The high efficiency (98.3%) minimises energy losses, reducing operational costs and supporting sustainable charging infrastructure. These attributes make the system suitable for large-scale EV fleets and weak grid conditions, enhancing grid stability and enabling cost-effective, scalable charging solutions for smart grid ecosystems.

Table 4 outlines the comparison analysis and shows that the suggested adaptive charging system outperforms traditional fixed-mode chargers. By incorporating real-time SOC and temperature feedback, the adaptive strategy enables dynamic transition between CC and CV modes, achieving faster charging with higher peak power delivery (up to 12 kW). The system also improves power quality, reducing grid current THD to 1.33% in G2V and 1.7% in V2G, ensuring compliance with IEEE 519 standards. Unlike traditional systems, which rely on passive thermal protection and fixed PI control, the proposed approach utilises a thermal model with current derating to minimise battery stress and extend cycle life. Additionally, the system offers enhanced charging efficiency (98.3%), full bidirectional operation and improved grid integration through an optimised LCL filter.

5. Conclusion

This paper proposed a novel adaptive charging strategy for a three-phase bidirectional on-board charger, aimed at enhancing battery life, optimising charging efficiency and ensuring grid compliance. The system integrates real-time SOC and temperature feedback through a unified control logic that adaptively transitions between CC and CV charging modes. A first-order thermal model is incorporated to monitor and manage battery temperature, thereby preventing thermal stress and prolonging battery health. The simulation results

Table 4. Comparative analysis of the proposed charging method to the existing charging methods.

Parameter	Existing charging systems	Proposed adaptive charging system	Reference(s)
Charging mode	Fixed CC/CV	Adaptive CC–CV with SOC and temperature feedback	Zdraveski et al. (2022), Etemesi et al. (2024) and Balasundar et al. (2021)
Charging power	7–10 kW	12 kW	Sethuraman and Rudhramoorthy (2024), Rivera et al. (2021) and Pradhan et al. (2023)
Charging time (20%–80% SOC)	6.5–8 h	5 h (reduced by 30%)	Hammerschmitt et al. (2024), Pradhan et al. (2023) and Rivera et al. (2021)
THD (grid current—G2V)	4%–5%	1.33%	Balasundar et al. (2021) and IEEE Standards Association (2014)
THD (grid current—V2G)	4.5%–5%	1.7%	Balasundar et al. (2021) and IEEE Standards Association (2014)
Control strategy	Fixed PI control without real-time adaptation	Adaptive controller with real-time SOC & temperature feedback	Etemesi et al. (2024)
Thermal management	Passive or external cooling-based cut-off	Real-time thermal model with current derating	Shahjalal et al. (2021)
Battery stress	High during fast charging (no thermal limit)	Reduced due to derating and smooth mode transitions	Zdraveski et al. (2022) and Etemesi et al. (2024)
Grid compliance	Limited harmonic mitigation	Enhanced via LCL filter	Han et al. (2020) and Balasundar et al. (2021)
Bidirectional operation (V2G)	Limited or not supported	Fully supported with control reversibility	Bera et al. (2022)
Charging efficiency	88%–95%	98.3%	Han et al. (2020) and Rivera et al. (2021)
Battery life span	Degrades with uncontrolled fast charging	Improved	Pradhan et al. (2023) and Levek and Steffan (2019)

CC, constant current; CV, constant voltage; G2V, grid-to-vehicle; SOC, state of charge; THD, total harmonic distortion; V2G, vehicle-to-grid.

demonstrated the efficacy of the proposed approach, achieving a charging efficiency of 98.3%, reducing charging time by approximately 30% and maintaining THD within IEEE 519 limits—1.33% in G2V and 1.7% in V2G modes. The system showed stable operation even under parameter variations, such as changes in grid-side inductance and voltage, validating its robustness. The key contributions of this work include (1) development of an adaptive controller integrating SOC and thermal feedback in real time, (2) mathematical modelling of AC–DC and DC–DC converter stages in the synchronous reference frame, (3) implementation of a thermal model with dynamic current derating based on predicted battery temperature, (4) validation of low THD, high efficiency and reduced charging time through MATLAB/Simulink (MathWorks, Inc.) simulation and (5) sensitivity analysis and robustness verification under grid disturbances and parameter deviations. The proposed charger provides a scalable, efficient and thermally safe charging solution suitable for future smart grid integration and electric mobility applications.

6. Limitations and Future Scope

The proposed system has certain limitations that warrant further development. Validation has been conducted in a simulation environment, which does not account for real-world factors such as load transients or communication delays. The thermal model is a simplified first-order system and may not capture the full complexity of battery heat dynamics during fast charging. The adaptive logic relies on precise SOC and temperature measurements, which may be difficult to obtain accurately in practical applications due to sensor inaccuracies or estimation errors. Future work will address these limitations through hardware-in-the-loop (HIL) testing using a dSPACE (dSPACE India Pvt. Ltd., Bangalore, India) real-time simulator under realistic grid conditions. The thermal model can be enhanced using data-driven or higher-order modelling approaches to improve accuracy. Integration of predictive control or machine learning-based adaptive tuning may further

improve robustness and real-time responsiveness. Additionally, expansion of the control architecture to support coordination among multiple EVs in a fleet, with load balancing and grid support capabilities, will improve scalability. These improvements will support deployment in real-world smart grid environments, ensuring better performance, adaptability and grid resilience.

References

Acharige, S. S. G., Haque, M. E., Arif, M. T., Hosseinzadeh, N., Hasan, K. N. and Oo, A. M. T. (2023). Review of Electric Vehicle Charging Technologies, Standards, Architectures, and Converter Configurations. *IEEE Transactions on Multidisciplinary*, 11, pp. 41218–41255. doi: 10.1109/ACCESS.2023.3267164

Ahmadi, A., Tavakoli, A., Jamborsalamati, P., Rezaei, N., Miveh, M. R., Gandoman, F. H., Heidari, A. and Nezhad, A. E. (2019). Power Quality Improvement in Smart Grids Using Electric Vehicles: A Review. *IET Electrical Systems in Transportation*, 9(2), pp. 53–64. doi: 10.1049/iet-est.2018.5023

Balasundar, C., Sundarabalan, C. K., Sharma, J., Srinath, N. S. and Guerrero, J. M. (2021). Design of Power Quality Enhanced Sustainable Bidirectional Electric Vehicle Charging Station in Distribution Grid. *Sustainable Cities and Society*, 74, p. 103242. doi: 10.1016/j.scs.2021.103242

Bera, T. K., Bohre, A. K., Ahmed, I., Bhattacharya, A. and Yadav, A. (2022). Smart Charging for Electric Vehicles (EVs): A Short Review. *IEEE Global Conference on Computing, Power and Communication Technologies*. New Delhi, India. doi: 10.1109/GlobConPT57482.2022.9938183

Danko, M., Adamec, J., Taraba, M. and Drgona, P. (2019). Overview of Batteries State of Charge Estimation Methods. *13th International Scientific Conference on Sustainable, Modern and Safe Transport*. pp. 186–192. doi: 10.1016/j.trpro.2019.07.029 (accessed date : 14 November 2022).

Etemesi, A. B. R., Megahed, T. F., Kanaya, H. and Mansour, D. E. A. (2024). Design of a Bidirectional EV Charger Using Unit Template-Based Current-Controlled Synchronous Reference Frame Hysteresis. *Journal of Electrical Engineering*, 75(1), pp. 29–40. doi: 10.2478/jee-2024-0005

Gong, L., Xiao, C., Cao, B. and Zhou, Y. (2018). Adaptive Smart Control Method for Electric Vehicle Wireless Charging System. *Energies*, 11, p. 2685. doi: 10.3390/en11102685

Hammerschmitt, B. K., Unsihuay-Vila, C., Sausen, J. P., Capeletti, M. B., Aoki, A. R., Teixeira, M. D., Barriquello, C. H. and da Rosa Abaide, A. (2024). Adaptive Charging Simulation Model for Different Electric Vehicles and Mobility Patterns. *Energies*, 17(16), p. 4032. doi: 10.3390/en17164032

Han, J., Zhou, X., Lu, S. and Zhao, P. (2020). A Three-Phase Bidirectional Grid-Connected AC/DC Converter for V2G Applications. *Journal of Control Science and Engineering*, 2020, pp. 1–12. doi: 10.1155/2020/8844073

Haque, M. R., Salam, K. M. A. and Razzak, M. A. (2023). A Modified PI-Controller Based High Current Density DC–DC Converter for EV Charging Applications. *IEEE Transactions on Multidisciplinary*, 11, pp. 27246–27266. doi: 10.1109/ACCESS.2023.3258181

IEEE Standards Association. (2014). IEEE Standard 519-2014: Recommended Practices and Requirements for Harmonic Control in Electric Power Systems.

Levek, V. and Steffan, P. (2019). Battery Lifespan Calculation and Principles of Design for Low Power Mode. *Journal of Electrical Engineering*, 70(1), pp. 39–45. doi: 10.2478/jee-2019-0005

Omkar, M. and Vijaya Kumar, M. (2024). Design of Filter for Single-Phase Bidirectional Battery Charger for Electrical Vehicle Applications. *International Journal on Electrical Engineering and Informatics*, 16(4), pp. 544–561. doi: 10.15676/ijeei.2024.16.4.3

Pradhan, R., Keshmiri, N. and Emadi, A. (2023). On-Board Chargers for High-Voltage Electric Vehicle Powertrains: Future Trends and Challenges. *IEEE Open Journal of Power Electronics*, 4, pp. 189–207. doi: 10.1109/OJPEL.2023.3251992

Rivera, S., Kouro, S., Vazquez, S., Goetz, S. M., Lizana, R. and Romero-Cadaval, E. (2021). Electric Vehicle Charging Infrastructure: From Grid to Battery. *IEEE Industrial Electronics Magazine*, 15, pp. 37–51. doi: 10.1109/MIE.2020.3039039

Sethuraman, R. and Rudhramoorthy, M. (2024). Performance of Bidirectional ON-Board Charger in Electric Vehicle: A Review. *e-Prime - Advances in Electrical Engineering, Electronics and Energy*, 8, p. 100613. doi: 10.1016/j.prime.2024.100613

Shahjalal, M., Shams, T., Islam, M. E., Alam, W., Modak, M., Hossain, S. B., Ramadesigan, V., Ahmed, M.

R., Ahmed, H. and Iqbal, A. (2021). A Review of Thermal Management for Li-ion Batteries: Prospects, Challenges, and Issues. *Journal of Energy Storage*, 39, p. 102518. doi: 10.1016/j.est.2021.102518

Thangavel, S., Mohanraj, D., Girijaprasanna, T., Raju, S., Dhanamjayulu, C. and Muyeen, S. M. (2023). A Comprehensive Review on Electric Vehicle: Battery Management System, Charging Station, Traction Motors. *IEEE Transactions on Multidisciplinary*, 11, pp. 20994–21019. doi: 10.1109/ACCESS.2023.3250221

Zdraveski, V., Angelov, J., Krstevski, P., Mateska, A. K., Vuletic, J. and Todorovski, M. (2022). Decentralized Controlled Charging and Vehicle-To-Grid Solution for Voltage Regulation in Low Voltage Distribution Systems. *Journal of Electrical Engineering*, 73(2), pp. 99–107. doi: 10.2478/jee-2022-0013